engineering proceedings

MDPI

Proceeding Paper

Surface Roughness Studies on F357 Aluminum Alloy Fabricated Using Laser Powder Bed Fusion Process †

Jaskaranpal Singh Dhillon *, Su Su, Oscar Sanchez Mata, Tejas Ramakrishnan and Mathieu Brochu *

REGAL Aluminum Research Center, Mining and Materials Engineering Department, McGill University, Wong Building, 3610 University St., Montreal, QC H3A 0C5, Canada

* Correspondence: jaskaranpal.dhillon@mail.mcgill.ca (J.S.D.); mathieu.brochu@mcgill.ca (M.B.)

† Presented at the 15th International Aluminium Conference, Québec, QC, Canada, 11–13 October 2023.

Abstract: Aluminum alloys processed using laser powder bed fusion are attracting industrial and research efforts striving to achieve the lightweighting potential and combination of good mechanical and corrosion properties. In this study, border parameter optimization for F357 (AlSi7Mg) alloy processed using LPBF was performed with the aim of reducing the as-fabricated surface roughness. The optimization revealed that laser power and scanning speed can significantly influence the surface roughness of cube vertical surfaces. Measured areal average surface roughness (S_a) for cube samples varied from 15 to 24 µm. The cube-based optimized parameters were used to fabricate angled wall samples with angles ranging from 45° to 90°. The surface roughness reduced when the built angle increased from 45° to 75°, while for 75–90°, the surface roughness values remained constant.

Keywords: LPBF; F357; surface roughness

1. Introduction

Laser powder bed fusion (LPBF) is an additive manufacturing technique in which parts are fabricated in a layer-by-layer approach by slicing a CAD model into defined layer thicknesses that are melted using a specific laser raster. LPBF allows for the fabrication of complex geometries, reduction in raw material wastage, and components with added functionalities for various industries such as aviation, aerospace, and medical, to name a few [1–3]. These are some advantages of LPBF which explain the scientific and industrial sectors' enthusiasm to further develop this fabrication process.

Aluminum (Al) alloys have been extensively studied for their good combination of lightweight, corrosion resistance, and higher specific strength. F357 (AlSi7Mg) is a beryllium-free variant of A357 alloy that is preferred to avoid the well-known toxicity issue related to this specific element [4,5]. LPBF was found compatible with F357 aluminum alloy since it is a near eutectic composition that results in a relatively small freezing range and has good fluidity [6]. LPBF-processed Al–Si-based alloys exhibit a peculiar microstructure with α-Al cells surrounded by an eutectic Si network [7–12]. This unique microstructure is the result of the rapid solidification environment [13].

The surface roughness of as-fabricated LPBF parts is higher than traditional processing methods such as machining, as reported in [14]. Thus, it is important to understand the variations in as-fabricated surface roughness and its influences on the performance of components. Previous studies [15–20] investigated the different aspects related to the surface roughness evolution of LPBF-processed AlSi10Mg aluminum alloy. The factors studied involved the influence of processing parameters such as laser power, scanning speed, scanning strategies, and overlap between tracks. These parameters govern the melt pool characteristics which in turn dictate the roughness evolution of the LPBF-processed parts. The stair-step effect, spattering, melt pool phenomena, morphology of solidified tracks, attachment of residual powder particles, and interaction between the adjacent tracks are among the underlying reasons for the higher surface roughness of LPBF-processed

Citation: Dhillon, J.S.; Su, S.; Sanchez Mata, O.; Ramakrishnan, T.; Brochu, M. Surface Roughness Studies on F357 Aluminum Alloy Fabricated Using Laser Powder Bed Fusion Process. *Eng. Proc.* **2023**, *43*, 8. https://doi.org/10.3390/engproc2023043008

Academic Editor: Houshang Alamdari

Published: 12 September 2023

parts [21]. Yuan et al. [22] studied the effect of laser scanning speed and reported that a higher scanning speed resulted in balling and instabilities, which resulted in a discontinuous morphology of the laser track. On the other hand, a lower scanning speed resulted in continuous and uniform laser weld track. Roughness occurs as a result of the physical interaction between the metal powder and the laser beam melting process [23]. The presence of overlapping regions in the neighboring tracks during processing results in a variation of linear surface roughness (R_a) when measured in different directions with respect to the laser scanning direction. Understanding the roughness is critical, as has been shown by Roach et al. [24]; the dimensional variations associated with surface morphology resulted in significant differences in the measured elongation to failure in tensile testing.

In the present work, light interferometry is used to study the effect of border scanning parameters and different printing orientations on the surface roughness of LPBF-processed F357 aluminum alloy.

2. Materials and Methods

The F357 aluminum alloy plasma atomized powder was supplied by Tekna Advanced Materials Inc (Sherbrooke, QC, Canada). Table 1 presents the composition of the as-received powder. A Microtrac Sync Particle Size analyzer was employed to determine the powder size distribution (PSD), which exhibited a D_{10} of 33 µm, a D_{50} of 42 µm, and a D_{90} of 56 µm, respectively. The powder particles were observed using a Hitachi SU3500 scanning electron microscope (SEM) to study particle morphology. Figure 1 shows SEM micrographs of powder particles, which reveals that the powder particles are spherical with only a few satellites.

Table 1. Chemical composition of F357 powder as per certificate of conformity provided by the manufacturer.

Element	Si	Mg	Fe	Ti	Mn	Zn	Cu	Be	Al
Wt %	6.7	0.5	0.06	0.1	0.006	0.01	<0.001	<0.0001	Balance

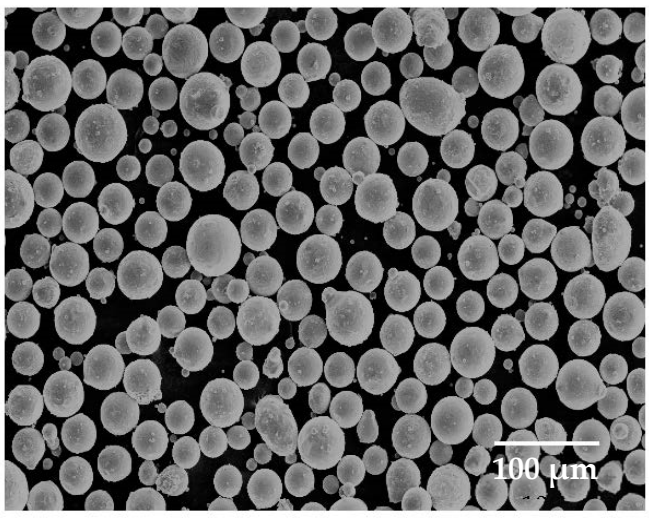

Figure 1. SEM micrographs of F357 powder.

The samples were fabricated using a Renishaw AM 400 LPBF system, equipped with a Nd-YAG laser, with a maximum power output of 400 W and a laser beam diameter of approximately 67 µm at focus. The fabrication was performed under an argon atmosphere to prevent the oxidation of parts. The oxygen level was maintained under 700 ppm during processing. The process used regular aluminum base plates as substrate. A scan rotation of 67° was employed between each layer. Eight cube samples were printed using a 60 µm layer thickness to optimize the border parameters. Table 2 presents the range of processing

parameters used for fabricating cubes and the formula used to calculate energy density. Figure 2a,b show the schematic of border and bulk of the samples. In addition, Figure 2a shows the sample position as a function of recoating direction and gas flow direction. In Figure 2b, the yellow arrow represents the building direction.

Table 2. Processing parameters for 60 µm layer thickness cube samples.

Layer Thickness (L_t) (µm)	Power (P) (W)	Scanning Speed (v) (mm/s)	Energy Density (E) (J/mm^2) $E = (P1000)/(v\ L_t)$
60	270–350	1000–1400	3.75–5.50

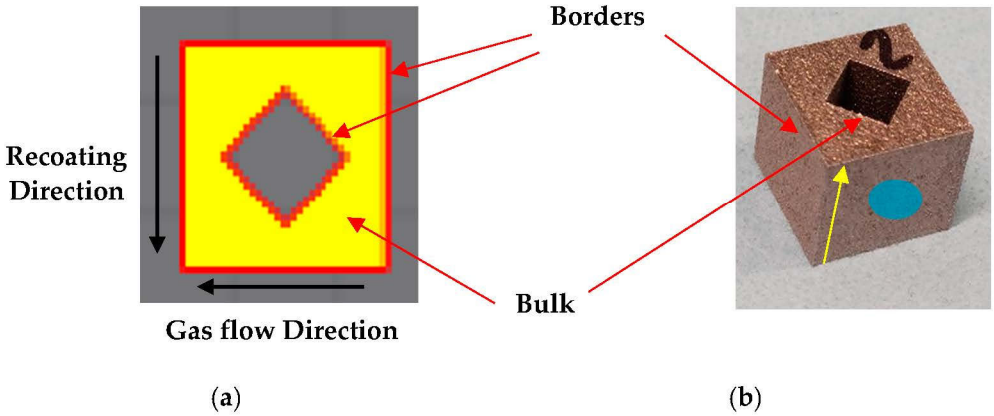

Figure 2. (**a**) Schematic showing borders of cube samples with diamond-shaped hole. The powder recoating and gas flow directions are also annotated. (**b**) LPBF-fabricated sample (yellow arrow shows the build direction, and blue marking depicts the side wall surface on which surface measurements were performed).

The optimized border parameters in terms of the lowest surface roughness determined from the cube study were used to fabricate angle walls with inclination angles varying from 45° to 90° with respect to the build direction for samples made with a layer thickness of 60 µm. Figure 3 shows the surfaces which will be referred to as upskin (upward-facing surface) and downskin (downward-facing surface). Figure 3 also shows the variation of wall angles from 45° to 90° with a step size of 5°. For surface roughness studies, the samples were removed from the build plate with a horizontal bandsaw. Further, the angle wall samples were sectioned using a hand hacksaw to study surface roughness for each individual inclination angle.

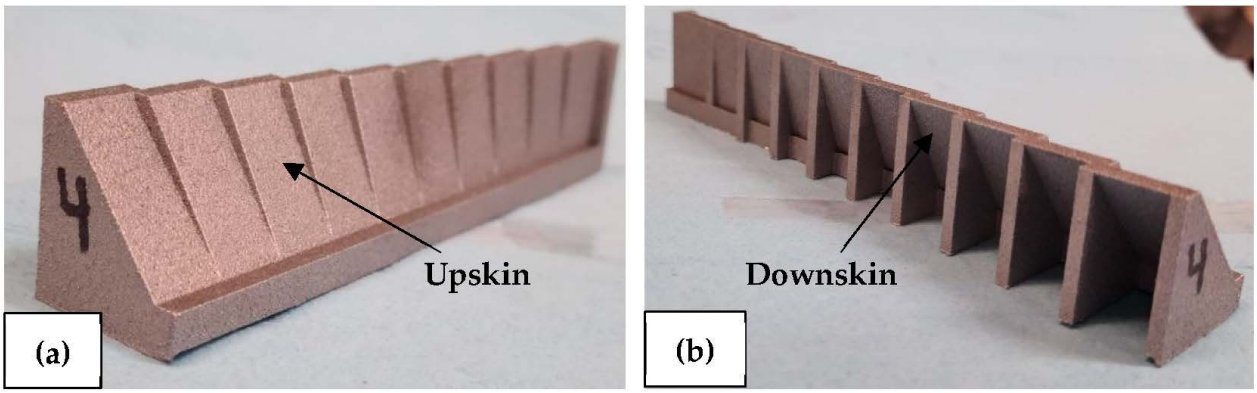

Figure 3. LPBF-fabricated angle walls showing (**a**) upskin and (**b**) downskin.

The surface topography was analyzed using ZYGO-3D optical surface profilometer on as-fabricated surfaces. For the cube samples, the surface roughness analysis was conducted on the marked side-wall surface of the cube, as indicated in Figure 2b with a blue circle. For the angle wall samples, both downskin and upskin surfaces of all inclination angles were scanned. Measurements were conducted using a 2.75x objective lens and a minimum surface area of 7 mm × 5 mm was scanned for each sample. Gaussian filter was used to extract the roughness data in accordance with ISO 21920-2:2021 guidelines [25]. A cut-off length equivalent to the D_{90} of the feedstock was used to solely incorporate the morphological features associated with partially melted particles [26]. Stitching with 20% overlap was utilized to ensure the analysis of most of the features of LPBF-processed specimen surface. In this study, the average areal surface roughness (S_a) is reported.

3. Results and Discussion

3.1. Surface Roughness Studies on Cube Samples

Figure 4 depicts the average areal surface roughness (S_a) variation with respect to energy density (E) for the 60 µm layer thickness samples. The highest and lowest values of S_a are 24 µm and 15 µm at energy densities of 3.75 J/mm^2 and 5.10 J/mm^2, respectively. The results indicate that the surface roughness of LPBF-processed parts can be controlled using appropriate process parameters. As depicted in Figure 4, the surface roughness decreases with an increase in energy density till 4.86 J/mm^2 and the values did not vary much for further increase in energy density within the analyzed range. This reduction can be attributed to the influence of the selected laser power and scanning speed, which in turn dictates the melt pool characteristics. Similar trends were reported in previous studies [15,20,27]. From the tested range of parameters, the optimal laser power and scanning speed, which lead to the lowest value of S_a, which is 15 µm, are 350 W and 1143 mm/s, respectively. These parameters are further used to fabricate angle wall samples at 60 µm layer thickness.

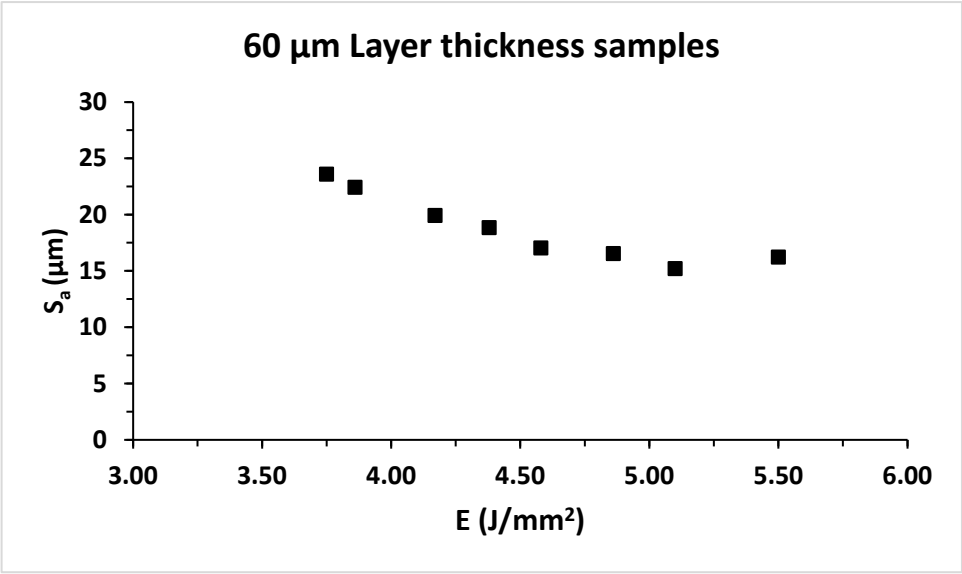

Figure 4. Variation of S_a with energy density (E) fabricated using 60 µm layer thickness samples.

It should be noted that continuing increase in energy density cannot guarantee a lower surface roughness value, as reported by Wang et al. [28], where an excessively high energy density can lead to defects such as keyhole and balling, which can increase surface roughness. The surface roughness of vertical walls in LPBF-fabricated samples can be attributed to aspects such as residual particles, which can be unmelted or partially melted particles that become adhered to the surface of melt pools because of heat concentrations at the end of laser tracks as the melt pool is surrounded by powder particles on one end

and bulk material on the other side. In that context, any factor affecting the melt pool characteristics, such as process parameters, powder layer thickness, and scanning strategies, will influence the roughness [15,20,21,29].

3.2. Surface Roughness Studies on Angle Wall Samples

Figure 5 indicates that the surface roughness decreases significantly with the increase in build angle, irrespective of whether the upskin or downskin surface is considered. Furthermore, Figure 5 also establishes that the downskin surface roughness is significantly higher in comparison to the respective upskin value aside from that for the build angles of 85° and 90°, where the surface roughness was similar. As shown in Figure 5, a similar trend for downskin can be found in roughness data from EOS GmbH for LPBF-processed F357 samples [30]. For the upskin surface, the S_a values decreased from 23 µm at 45° to 15 µm at 80°. With a further increase in wall angle, the surface roughness value did not differ much. For the downskin surface, a maximum value of 33 µm was observed at 45° and a minimum value of 16 µm was observed at 90°. This variation in surface roughness indicates that the surface quality of a part will be impacted by the inclination angle with respect to the substrate. The S_a value at a 90° build angle is similar to the side wall roughness of the 60 µm cube sample.

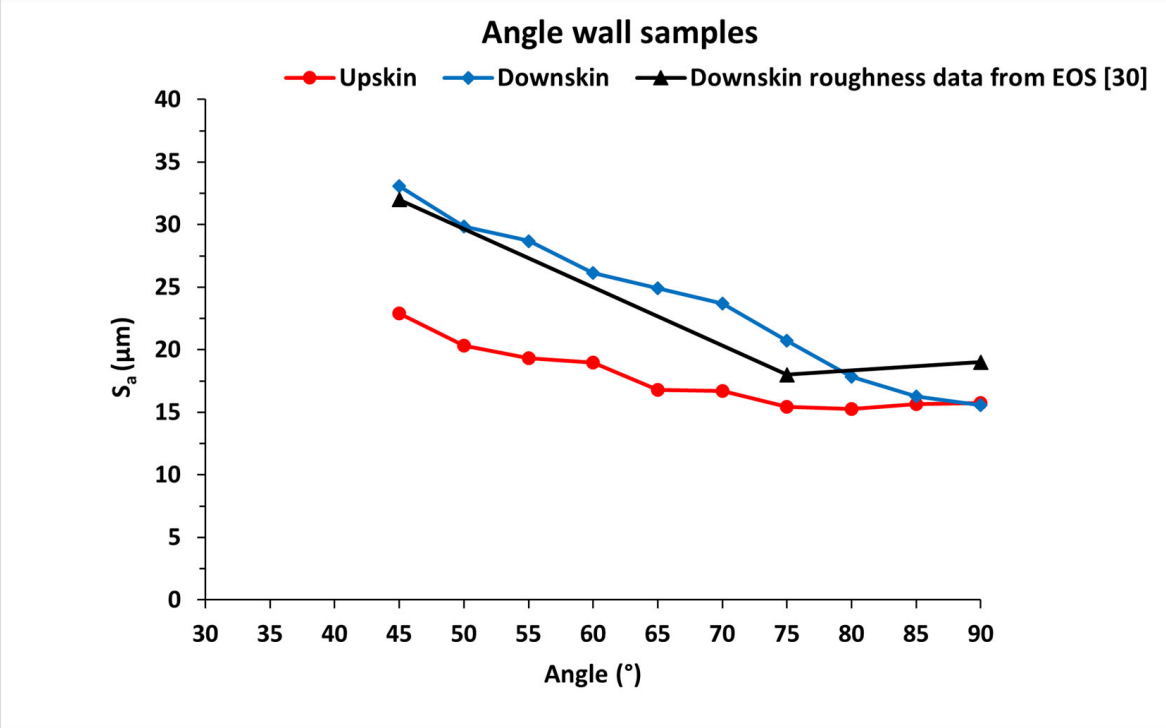

Figure 5. Influence of build angles on surface roughness of upskin and downskin surfaces [30].

The upskin roughness is dictated by the stair-step effect and, in some cases, the spatter particles. During the fabrication of angled walls, the length of the overhang, which can influence the surface roughness, closely relates to the powder layer thickness and inclination angle, as reported by Yang et al. [20]. It was reported that the overhang length increases with a reduction in the build angle. This was considered as one of the reasons why an increase in surface roughness at the lower build angles was observed. The higher surface roughness of the downskin can be attributed to the phenomenon mentioned above as it results in residual powder particles or partially melted particles adhering to the bottom surface during the solidification of the melt pool, which contributes to the surface roughness of downskin surfaces [31]. When the laser beam interacts with the powder bed at the borders, the solidified bulk material provides support to the molten pool on

one side while the melt pool remains in contact with the powder on the other side. With increase in build angle, the portion of the solid layer that supports molten pool increases, and the corresponding melt pool area where the powder particles can adhere decreases, thus lowering the surface roughness at higher build angles [20]. The presence of interlayer powder particles, melt pool characteristics, and process parameters are important factors that govern the upskin and downskin surface roughness.

4. Conclusions

F357 aluminum alloy cubes and angle wall samples were fabricated using the LPBF process and their surface roughness was investigated. Based on the combination of process parameters and procedures used in this work, the following main conclusions can be drawn:

For the cube samples, the surface roughness decreased with an increase in energy density. The lowest observed surface roughness was 15 µm for the cube sample fabricated using 350 W laser power and 1143 mm/s scanning speed.

For angle walls, the upskin surface roughness reduced with an increase in build angle from 23 µm at 45° to 15 µm at 80°. For the downskin surfaces, a similar trend followed, as the surface roughness, which was 33 µm at 45°, reduced to 16 µm at 90°.

Upskin exhibited lower surface roughness values compared to downskin surfaces for their respective inclination angles, aside from 90° as surfaces are vertical at 90°.

Author Contributions: Conceptualization, J.S.D. and M.B.; Investigation, J.S.D. and S.S.; Formal analysis, J.S.D. and O.S.M.; Data curation, J.S.D. and S.S.; Writing—original draft, J.S.D.; Writing—review and editing, J.S.D., O.S.M., T.R. and M.B.; Methodology, O.S.M. and T.R.; Resources, M.B.; Supervision, M.B.; Funding acquisition, M.B.; Project administration, M.B. All authors have read and agreed to the published version of the manuscript.

Funding: This research received financial support from the Natural Sciences and Engineering Research Council of Canada (NSERC; project number: CRDPJ 541425–19).

Institutional Review Board Statement: Not applicable.

Informed Consent Statement: Not applicable.

Data Availability Statement: The authors do not have permission to share data.

Acknowledgments: The authors want to thank Richard Chromik for providing access to ZYGO 3D optical surface profilometer and would also like to thank Angelica Ivonne Valencia Ruiz for the help with the printing of the F357 aluminum alloy samples.

Conflicts of Interest: The authors declare that they have no known competing financial interests or personal relationships that could have appeared to influence the work reported in this paper.

References

1. DebRoy, T.; Wei, H.L.; Zuback, J.S.; Mukherjee, T.; Elmer, J.W.; Milewski, J.O.; Beese, A.M.; Wilson-Heid, A.; De, A.; Zhang, W. Additive manufacturing of metallic components–Process, structure and properties. *Prog. Mater. Sci.* **2018**, *92*, 112–224. [CrossRef]
2. Aboulkhair, N.T.; Simonelli, M.; Parry, L.; Ashcroft, I.; Tuck, C.; Hague, R. 3D printing of Aluminium alloys: Additive Manufacturing of Aluminium alloys using selective laser melting. *Prog. Mater. Sci.* **2019**, *106*, 100578. [CrossRef]
3. Chou, S.; Trask, M.; Danovitch, J.; Wang, X.; Choi, J.; Brochu, M. Pulsed laser powder bed fusion additive manufacturing of A356. *Mater. Charact.* **2018**, *143*, 27–33. [CrossRef]
4. Esposito, L.; Bertocco, A.; Cricrì, G.; Rosiello, V. Welding-repair effect on F357-T6 aluminum castings: Analysis of fatigue life. *Int. J. Adv. Manuf. Technol.* **2019**, *102*, 3699–3706. [CrossRef]
5. Nickels, L. AM behind the scenes. *Met. Powder Rep.* **2017**, *72*, 168–171. [CrossRef]
6. Kotadia, H.; Gibbons, G.; Das, A.; Howes, P. A review of Laser Powder Bed Fusion Additive Manufacturing of aluminium alloys: Microstructure and properties. *Addit. Manuf.* **2021**, *46*, 102155. [CrossRef]
7. Ming, X.; Song, D.; Yu, A.; Tan, H.; Zhang, Q.; Zhang, Z.; Chen, J.; Lin, X. Effect of heat treatment on microstructure, mechanical and thermal properties of selective laser melted AlSi7Mg alloy. *J. Alloys Compd.* **2023**, *945*, 169278. [CrossRef]
8. Tonelli, L.; Liverani, E.; Morri, A.; Ceschini, L. Role of Direct Aging and Solution Treatment on Hardness, Microstructure and Residual Stress of the A357 (AlSi7Mg0.6) Alloy Produced by Powder Bed Fusion. *Metall. Mater. Trans. B* **2021**, *52*, 2484–2496. [CrossRef]

9. Cheng, C.C.; Li, Z.; Dhillon, J.S.; Hudon, P.; Brochu, M. Influence of powder layer thickness on microstructure and T5 heat treatability of F357 alloy fabricated by laser powder bed fusion process. *J. Alloys Compd.* **2023**, *948*, 169633. [CrossRef]
10. Wang, M.; Song, B.; Wei, Q.; Zhang, Y.; Shi, Y. Effects of annealing on the microstructure and mechanical properties of selective laser melted AlSi7Mg alloy. *Mater. Sci. Eng. A* **2018**, *739*, 463–472. [CrossRef]
11. Casati, R.; Coduri, M.; Checchia, S.; Vedani, M. Insight into the effect of different thermal treatment routes on the microstructure of AlSi7Mg produced by laser powder bed fusion. *Mater. Charact.* **2021**, *172*, 110881. [CrossRef]
12. Li, Z.; Cheng, C.C.; Dhillon, J.S.; Kwon, S.Y.; Hudon, P.; Brochu, M. Precipitation behavior of an Al7SiMg alloy processed by laser powder bed fusion during non-isothermal and isothermal heat treatments. *Materialia* **2023**, *28*, 101751. [CrossRef]
13. Tang, M.; Pistorius, P.C.; Narra, S.P.; Beuth, J.L. Rapid Solidification: Selective Laser Melting of AlSi10Mg. *JOM* **2016**, *68*, 960–966. [CrossRef]
14. European Powder Metallurgy Association (EPMA)—Introduction to Additive Manufacturing Technology (Brochure). Available online: https://www.epma.com/epma-free-publications/product/introduction-to-additive-manufacturing-brochure (accessed on 25 April 2023).
15. Li, B.-Q.; Li, Z.; Bai, P.; Liu, B.; Kuai, Z. Research on Surface Roughness of AlSi10Mg Parts Fabricated by Laser Powder Bed Fusion. *Metals* **2018**, *8*, 524. [CrossRef]
16. Bailey, C.M.; Morrow, J.A.; Stallbaumer-Cyr, E.M.; Weeks, C.; Derby, M.M.; Thompson, S.M. Effects of Build Angle on Additively Manufactured Aluminum Alloy Surface Roughness and Wettability. *J. Manuf. Sci. Eng.* **2022**, *144*, 081010. [CrossRef]
17. Yang, T.; Liu, T.; Liao, W.; MacDonald, E.; Wei, H.; Chen, X.; Jiang, L. The influence of process parameters on vertical surface roughness of the AlSi10Mg parts fabricated by selective laser melting. *J. Mater. Process. Technol.* **2019**, *266*, 26–36. [CrossRef]
18. Mirabal, A.; Loza-Hernandez, I.; Clark, C.; Hooks, D.E.; McBride, M.; Stull, J.A. Roughness measurements across topographically varied additively manufactured metal surfaces. *Addit. Manuf.* **2023**, *69*, 103540. [CrossRef]
19. Beevers, E.; Brandão, A.D.; Gumpinger, J.; Gschweitl, M.; Seyfert, C.; Hofbauer, P.; Rohr, T.; Ghidini, T. Fatigue properties and material characteristics of additively manufactured AlSi10Mg–Effect of the contour parameter on the microstructure, density, residual stress, roughness and mechanical properties. *Int. J. Fatigue* **2018**, *117*, 148–162. [CrossRef]
20. Yang, T.; Liu, T.; Liao, W.; Wei, H.; Zhang, C.; Chen, X.; Zhang, K. Effect of processing parameters on overhanging surface roughness during laser powder bed fusion of AlSi10Mg. *J. Manuf. Process.* **2021**, *61*, 440–453. [CrossRef]
21. Leary, M.; Khorasani, M.; Sarker, A.; Tran, J.; Fox, K.; Downing, D.; Du Plessis, A. Surface roughness. In *Fundamentals of Laser Powder Bed Fusion of Metals*; Yadroitsev, I., Yadroitsava, I., du Plessis, A., MacDonald, E., Eds.; Elsevier: Amsterdam, The Netherlands, 2021; pp. 179–213. [CrossRef]
22. Yuan, W.; Chen, H.; Cheng, T.; Wei, Q. Effects of laser scanning speeds on different states of the molten pool during selective laser melting: Simulation and experiment. *Mater. Des.* **2020**, *189*, 108542. [CrossRef]
23. Lou, S.; Jiang, X.; Sun, W.; Zeng, W.; Pagani, L.; Scott, P. Characterisation methods for powder bed fusion processed surface topography. *Precis. Eng.* **2019**, *57*, 1–15. [CrossRef]
24. Niu, H.; Chang, I. Instability of scan tracks of selective laser sintering of high speed steel powder. *Scr. Mater.* **1999**, *41*, 1229–1234. [CrossRef]
25. ISO 21920-2:2021—Geometrical Product Specifications (GPS)—Surface Texture: Profile—Part 2: Terms, Definitions and Surface Texture Parameters. Available online: https://webstore.ansi.org/standards/iso/iso219202021-2458825 (accessed on 4 May 2023).
26. Ghosh, A. *Surface Morphological Effects of Laser Powder Bed Fusion and Laser Micromachining in Micro-Scale Parts*; McGill University: Montréal, QC, Canada, 2021.
27. Gockel, J.; Sheridan, L.; Koerper, B.; Whip, B. The influence of additive manufacturing processing parameters on surface roughness and fatigue life. *Int. J. Fatigue* **2019**, *124*, 380–388. [CrossRef]
28. Wang, L.-Z.; Wang, S.; Wu, J.-J. Experimental investigation on densification behavior and surface roughness of AlSi10Mg powders produced by selective laser melting. *Opt. Laser Technol.* **2017**, *96*, 88–96. [CrossRef]
29. Qiu, C.; Panwisawas, C.; Ward, M.; Basoalto, H.C.; Brooks, J.W.; Attallah, M.M. On the role of melt flow into the surface structure and porosity development during selective laser melting. *Acta Mater.* **2015**, *96*, 72–79. [CrossRef]
30. EOS Aluminium AlF357 Material Data Sheet Metal Solutions. Available online: https://www.eos.info/03_system-related-assets/material-related-contents/metal-materials-and-examples/metal-material-datasheet/aluminium/material_datasheet_eos_aluminium_alf357_premium_en.pdf (accessed on 4 May 2023).
31. Wang, D.; Yang, Y.; Yi, Z.; Su, X. Research on the fabricating quality optimization of the overhanging surface in SLM process. *Int. J. Adv. Manuf. Technol.* **2013**, *65*, 1471–1484. [CrossRef]